RSC Advances

ROYAL SOCIETY OF CHEMISTRY

www.rsc.org/advances

Journal Name

ARTICLE

Synthesis of $Zn_3V_2O_8$ nanoplatelets for lithium-ion battery and supercapacitor applications

Received 00th January 20xx,
Accepted 00th January 20xx

DOI: 10.1039/x0xx00000x

www.rsc.org/

Subbukalai Vijayakumar, Seong-Hun Lee, Kwang-Sun Ryu*

$Zn_3V_2O_8$ nanoplatelets were successfully synthesized using a hydrothermal method. Formation of the $Zn_3V_2O_8$ nanoplatelets was explained through splitting, exfoliation and self-aggregation mechanisms. FESEM revealed nanoplatelet morphology with thickness of 27.9 nm. HRTEM imaging confirmed the crystalline nature of the $Zn_3V_2O_8$ nanoplatelets, and the SAED pattern clearly indicated the prepared sample to be $Zn_3V_2O_8$. The prepared $Zn_3V_2O_8$ nanoplatelets were further studied for their potential application in Li-ion batteries and supercapacitors. The discharge capacity of the second cycle was 558 mA h g^{-1} at 100 mA g^{-1}. The $Zn_3V_2O_8$ nanoplatelets exhibited a maximum specific capacitance of 302 F g^{-1} at a scan rate of 5 mV s^{-1}. Furthermore, the $Zn_3V_2O_8$ electrode retained about 98 % of its initial specific capacitance after 2000 cycles. The described $Zn_3V_2O_8$ nanoplatelets were found to be a highly suitable electrode material for energy storage applications.

Introduction

The growing concerns about global warming and ever-increasing crude oil prices due to our dependency on fossil fuels has brought about a rapid development of renewable energy sources and an ever increasing interest in advanced energy storage devices.[1] Lithium-ion batteries (LIBs) and supercapacitors (SCs) are important electrical energy storage devices. LIBs and SCs highly suitable for use in portable electronic devices, hybrid electric vehicles (HEVs) and large scale electric networks.[2] Hence, the development of energy storage devices, including supercapacitors and lithium ion batteries, has received considerable interest from researchers in recent years. Supercapacitors have a higher power density than conventional batteries, whereas conventional batteries have a higher energy density than capacitors and supercapacitors. [3] The high power output of supercapacitors is useful in hybrid electric vehicles, which use lithium-ion batteries to supply high power during acceleration. Such systems can also be applied to recover the energy which would otherwise be lost during braking.[3]

Transition metal oxides are an important class of functional materials which have been widely used as electrode materials within energy storage devices, especially in supercapacitors and lithium-ion batteries.[4] Recently, it has been shown that a number of mixed transition metal oxides are promising candidates for energy storage devices, such as lithium-ion batteries and electrochemical supercapacitors. The mixed transition metal oxides can deliver rich redox reactions in electrochemical reactions due to the coexistence of two different metal species within a single crystal structure.[5] Recently, metal vanadates have been applied as electrode materials within supercapacitors and lithium-ion batteries.[6-12] Nickel vanadate on nickel foam was studied as an electrode material for supercapacitors by Zhang *et al.*[6] They reported the retention of 66.7 % capacitance after 5000 cycles. Zhang *et al.* [9] reported first and second discharge capacities of 875.8 and 472.4 mA h g^{-1}, respectively, at a current density of 100 mA g^{-1}, for MnV_2O_6 nanobelt anodes. Similarly, Xiao *et al.*[10] reported an initial reversible capacity of 548 mA h g^{-1} for ZnV_2O_4 hollow microspheres.

Zinc vanadates ($Zn_3V_2O_8$ nanomaterials) have been extensively studied for their energy storage and photo catalytic applications. However, there has been far less interest in their optical, photocatalytic and energy storage applications. Very few attempts have been made to explore the photonic [13], photocatalytic [14] or lithium-ion battery applications of $Zn_3V_2O_8$ nanomaterials. [15,16] To best of our knowledge, there have not been any previously published studies of the supercapacitor performance of $Zn_3V_2O_8$ nanomaterials. Hence, we made an attempt to synthesis $Zn_3V_2O_8$ nanomaterials and study their electrode performance in order to determine their suitability for application within supercapacitors.

In this work, we report the synthesis of $Zn_3V_2O_8$ nanoplatelets by a hydrothermal method using sodium dodecyl sulfate as a surfactant. The structural and morphological features of the prepared $Zn_3V_2O_8$ nanoplatelets were characterized using FESEM and HR-TEM. The possible formation mechanism of platelet structure, as well as the $Zn_3V_2O_8$ nanoplatelets application within lithium-ion batteries and supercapacitors, is reported and discussed in detail.

Department of Chemistry and Energy Harvest Storage Research Center (EHSRC), University of Ulsan, Muger-dong, Nam-gu, Ulsan 680-749, Republic of Korea.
Email: ryuks@ulsan.ac.kr (K.-S. Ryu). Tel: 82-52-259-2763 Fax: 82-52-259-2348

Electronic Supplementary Information (ESI) available: XRD pattern of $Zn_3V_2O_8$ precursor sample, BET isotherm of $Zn_3V_2O_8$ and scan rate versus peak current curve. See DOI: 10.1039/x0xx00000x

Experimental details

Synthesis of $Zn_3V_2O_8$ nanoplatelets

The typical synthesis of $Zn_3V_2O_8$ nanoplatelets was carried out as follows: 0.8651 g of sodium dodecyl sulfate (SDS) was dissolved in 25 ml of water. 0.4679 g of ammonium metavanadate and 0.5949 g of zinc nitrate hexahydrate were then dissolved in 25 ml of water, and were added to the SDS solution. 0.4 g of 10 ml of NaOH was then added to the above mixture and stirred continuously for a period of 15 min. The final solution was transferred to a100 ml Teflon lined autoclave vessel, and was maintained at 180 ºC for 24 h. The autoclave was then allowed to cool to room temperature and the final precipitate was collected by centrifugation, followed by washing of water and ethanol. Finally, the collected precipitate was dried at 80 ºC and calcined at 400 ºC for 1 h in air at a heating rate of 5 ºC per min.

Material characterization:

Thermogravimetric analysis of the sample was carried out by using a thermogravimetric analyzer (TGA, Q50, TA Instruments, New Castle, DE, USA). X-ray diffraction (XRD) was carried out using a Rigaku-Ultima 4 X-ray diffractometer. X-ray photo electron spectroscopy (XPS) was performed using a Thermo scientific with a Al K alpha X-ray source. A morphological study of the synthesized nanomaterial was carried out using a field emission scanning electron microscope (FESEM) (Jeol-JSM6500F and Jeol-JSM7600F). AFM measurement was carried out using VEECO DI-3100 instrument. High resolution transmission electron microscopy (HRTEM) and selected area electron diffraction (SAED) were carried out using a Jeol JEM-2100F. The N_2 adsorption-desorption measurement was carried out on a nanoPOROSITY-XQ Instrument using the Brunauer-Emmett-Teller (BET) gas adsorption method.

Electrochemical measurements:

The $Zn_3V_2O_8$ nanoplatelets anode was prepared using an active material, a conductive agent (super P) and a binder (PVDF) with a respective ratio of 80:10:10. Test cells (CR2032) were assembled in an argon filled glove box, using $Zn_3V_2O_8$ nanoplatelets coated on copper foil as the anode, Li foil as the cathode, and Celgard 3501 as the separator. The electrolyte solution was 1.0 M $LiPF_6$ (dissolved in ethylene carbonate (EC) and diethylene carbonate (DEC)). Cell performance was measured using a WonATech WBCS3000 battery tester. The working electrode for supercapacitor measurements was prepared as follows: 70 wt % of $Zn_3V_2O_8$ nanoplatelets and 25 wt% of carbon black (super P) was mixed using a mortar and pestle. Polytetrafluro-ethylene (PTFE) (5 wt%) was added to this mixture to form a slurry, which was then coated on an area of 1 cm^2 of nickel foam and was dried overnight at 80 °C. An IVAMSTAT instrument was used to determine supercapacitor performance. A saturated calomel electrode (SCE) and platinum wire were used as the reference and counter electrode, respectively. The electrochemical properties were analyzed using 6.0 M KOH as the electrolyte.

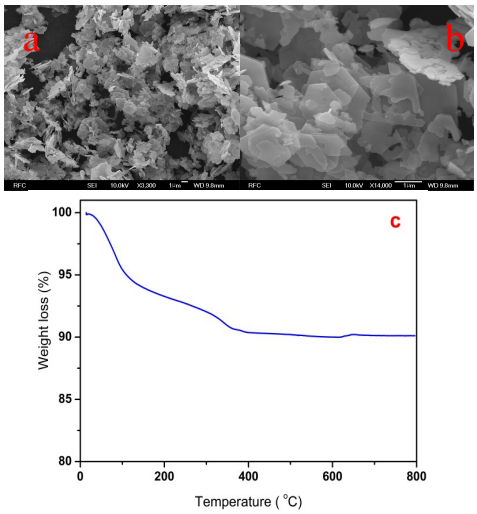

Fig.1. (a,b) FESEM images and (c) TGA curve of precursor sample

Results and Discussions

Zinc vanadate nanoplatelets were synthesized via a hydrothermal method using SDS as a surfactant. The morphology of the prepared sample was characterized by field emission scanning electron microscopy. The image of the zinc vanadate sample reveled nanoplatelet morphology, as shown in figs 1a and 1b. The platelets were well distributed at different dimensions. The thickness of the platelets was small. The XRD pattern of the precursor sample was shown in Fig. S1. All the diffraction peaks except 18.7 and 56.9 can be indexed to $Zn_3V_2O_7(OH)_2.2H_2O$ (JCPDS No: 87-0417). The remaining peaks can be indexed to $Zn_3V_2O_8$ (JCPDS No: 34-0378). Thermal studies were carried out in order to determine the thermal stability and decomposition profile of the sample. Fig. 1c shows the thermogravimetric curve of the sample. The major weight loss, occurring below 400 °C, was about 10 %, and was attributed to the loss of adsorbed and coordinated water. [17] There was no considerable weight loss between 400 °C and 800 °C. Based on the TGA result, the prepared sample was calcined at 400 °C for 1 h at a heating rate of 5 °C per min. The X-ray diffraction pattern of the calcined sample was recorded from 10 to 80 ° and is presented in fig. 2. All diffraction peaks were indexed to $Zn_3V_2O_8$ (JCPDS no. 34-0378). The nonexistence of other peaks corroborated the purity of the prepared material.

The purity and oxidation state of $Zn_3V_2O_8$ nanoplatelets were characterized by using X-ray photo electron spectroscopy (XPS). Fig.3a shows the complete survey spectrum of the $Zn_3V_2O_8$ nanoplatelets. It shows the presence of V2p, O1s, C1s, and Zn2p states. Fig. 3b represents the Zn2p spectrum. The two peaks in the Zn2p spectrum at 1021.58 and 1044.68 eV correspond to $Zn2p_{3/2}$ and $Zn2p_{1/2}$.[18] The V2p spectrum is shown in fig.3c. The peak positions at 516.78($V2p_{3/2}$) and 524.38 eV ($V2p_{1/2}$) were attributed to the V^{5+} state.[19] Fig.3d shows the XPS spectrum of O 1s. The O 1s

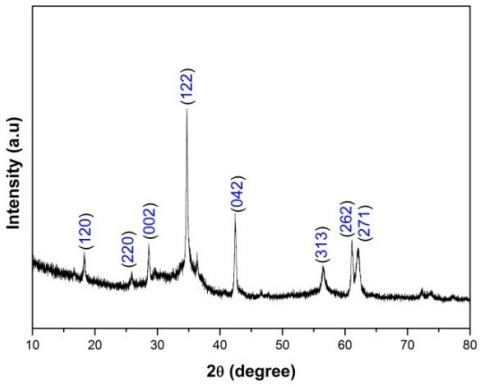

Fig.2. XRD pattern of $Zn_3V_2O_8$ nanoplatelets

spectrum was deconvoluted into three components (O1, O2, and O3), with binding energies of 529.58, 531.0 and 532.4 eV, respectively. The O1 peak at 529.58 eV was attributed to a metal-oxygen bond, i.e. V-O binding of ZnV_2O_8.[20] The O2 peak at 531.0 eV was attributed to a large number of defect sites with minimum oxygen coordination and small particle size.[21] The O3 components at the higher binding energy of 532.4 eV correspond to chemically and physically bonded water within the surface.[21]

Fig. 4 (a-c) present the FESEM images of $Zn_3V_2O_8$ nanomaterials at different magnifications. The FESEM images of the prepared $Zn_3V_2O_8$ nanomaterials show the nanoplatelets morphology. Figs. 4a and b clearly shows the even distribution of nanoplatelets with a flake like arrangement. Fig. 4c depicts the nanoplatelets morphology and dimensions. The platelets are arranged with spacing between neighboring nanoplatelets, which offers an effective electron and ion transport and supports the improvement of electrochemical performance in batteries and supercapacitors. The length of the nanoplatelets is about 1 µm and the breath is between 500 nm to 1 µm.

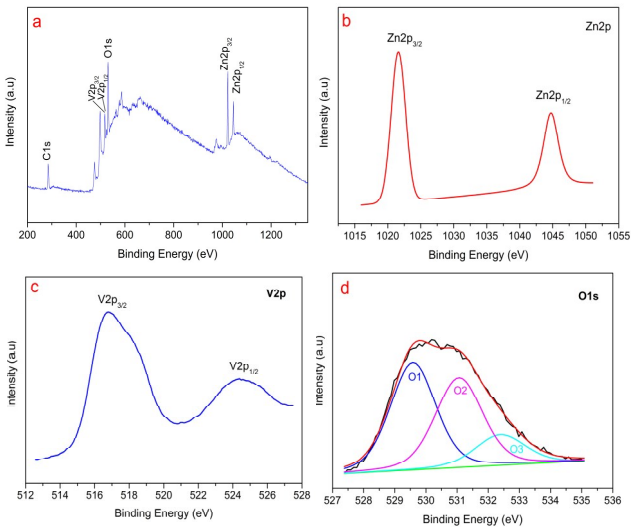

Fig.3. XPS spectra of (a) Survey scan (b) Zn2p, (c) V2p, and (d) O1s for $Zn_3V_2O_8$ nanoplatelets

Fig. 4d shows the AFM image of zinc vanadate nanoplates. The thickness of the nanoplatelets measured from AFM is 27.9 nm. The structure of the $Zn_3V_2O_8$ nanoplatelets was further characterized using HRTEM. Fig. 4(e,f) shows HRTEM images of $Zn_3V_2O_8$ nanoplatelets. TEM images clearly revealed the nanoplatelet arrangement and dimensions. Fig. 4g shows the higher magnification HRTEM image. The image clearly shows the crystalline structure of the sample. The d-spacing corresponds with a plane (271) of $Zn_3V_2O_8$. Fig. 4h presents the selected area electron diffraction (SAED) pattern of $Zn_3V_2O_8$ nanoplatelets. The SAED pattern can be indexed to $Zn_3V_2O_8$.

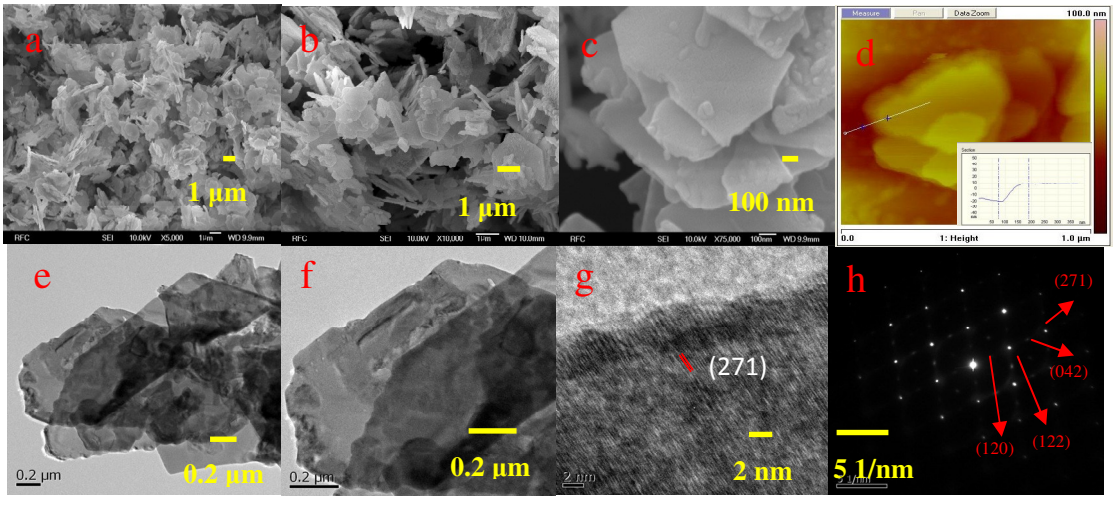

Fig.4 (a-c) FESEM images of $Zn_3V_2O_8$ nanoplatelets at different magnifications, (d) AFM image of $Zn_3V_2O_8$ nanoplatelets, (e, f and g) HRTEM images of $Zn_3V_2O_8$ nanoplatelets, and (h) SAED pattern of $Zn_3V_2O_8$ nanoplatelets.

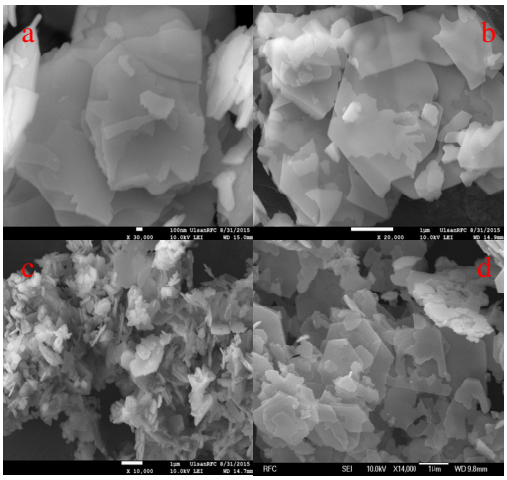

Fig. 5. FESEM images of $Zn_3V_2O_8$ precursor sample at different hydrothermal duration, (a) 6 h, (b) 12 h, (c) 18 h, and (d) 24 h.

Time dependent experiment has been carried out to explain the formation of nanoplateletes. Fig. 5 shows the FESEM images of precursor sample prepared at different duration of hydrothermal treatment. A formation mechanism of the $Zn_3V_2O_8$ nanoplatelets based on the time-dependent experiment results are presented in fig.6. The formation of $Zn_3V_2O_8$ nanoplatelets includes nucleation, growth, splitting and exfoliation processes, as well as self-aggregation. Initially, zinc and vanadium ions react to form zinc vanadate nuclei. After nucleation, the growth process starts to form a Zinc vanadate nanostructure. Here, the role of SDS is important. SDS acts as a structure directing agent that controls the surface free energy.[22] Hence, it enhances the growth process. The structure of the final product is dependent upon hydrothermal temperature, duration, concentration of the surfactant and pH of the solution, etc. Initially, thick zinc vanadate platelets are formed. As the hydrothermal reaction continues, the platelets are split into thin sheets.[19]

Fig. 5a shows (after 6 h of hydrothermal reaction) the thick nanoplates with sheets. These sheets are formed may due to splitting process. The splitting process continued up to 12 hours of hydrothermal treatment (Fig. 5b). The sheets are then exfoliated to form thin platelets (Fig. 5c).[19] After exfoliation, the sheets are attached together by self-aggregation, forming the Zinc vanadate nanoplatelets (Fig. 5d).

The $Zn_3V_2O_8$ nanoplatelets were employed to BET measurement to know the details of specific surface area and pore size distribution. Fig. S2 shows the BET isotherm and corresponding pore size distribution curve of $Zn_3V_2O_8$ nanoplatelets. The BET surface area of the $Zn_3V_2O_8$ nanoplatelets is 11.53 m^2 g^{-1}. The pore size distribution curve for the adsorption by BJH method clearly indicates that most of the pores are available in the region of 2 – 10 nm. The mean pore diameter of the $Zn_3V_2O_8$ nanoplatelets is 5.9 nm. The high surface area with porous nature helps to enhance the diffusion of ions which improve the electrochemical performance in both Li-ion batteries and supercapacitors [23].

The electrochemical performance of $Zn_3V_2O_8$ nanoplatelets was studied using cyclic voltammetry and charge-discharge analysis, and their potential as the active material for lithium-ion batteries was determined. Fig. 7a shows the CV curves of $Zn_3V_2O_8$ nanoplatelets in the potential range of 0.01 to 3.0 V at a scan rate of 0.1 mV s^{-1}. The cathodic scan of the CV curve shows reduction peaks at 0.59 is due to a reduction of zinc (Zn^{2+} to Zn^0) and reduction of vanadium (V^{5+} to V^{4+} and further to V^{3+}) .[16, 24] The oxidation peak at 1.23 is due to the oxidation of vanadium (V^{3+} to V^{5+}) and zinc (Zn^0 to Zn^{2+}). The charge-discharge measurement of $Zn_3V_2O_8$ nanoplatelets was carried out using a potential range of 0.01 to 3.0 V at a current density of 100 mA g^{-1}. Fig. 7b shows the charge-discharge profile of $Zn_3V_2O_8$ nanoplatelets at cycles 1, 2, 3, 10, 20, 30 and 40. The discharge curve of first cycle is different from the subsequent cycles. It shows a plateau at about 1.1 to 0.19 V. The capacity of first cycle plateau at lowers than 0.19 V is due to slow lithium storage process into the orthorhombic type $Zn_3V_2O_8$ and plateau at higher voltage can be attributed to a Faradic nature of the material.[16]

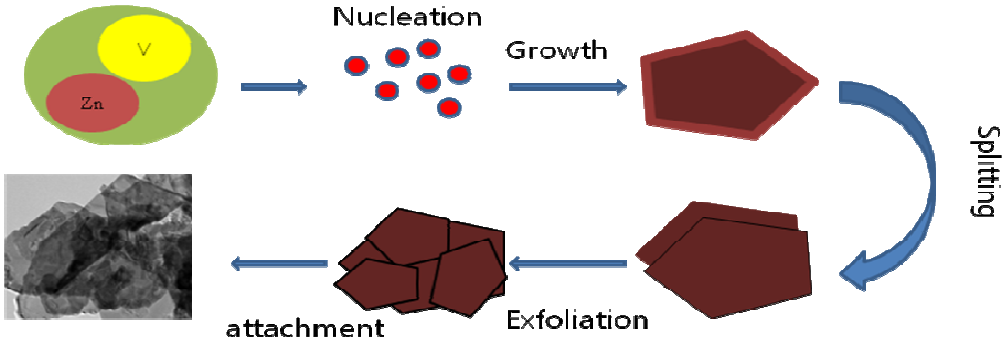

Fig.6. Schematic representation of the formation of $Zn_3V_2O_8$ nanoplatelets

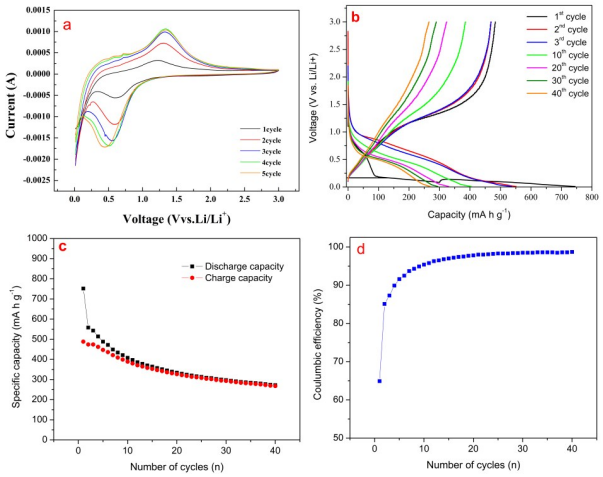

Fig.7. (a) CV curves of $Zn_3V_2O_8$ at a scan rate of 0.1 mV s^{-1} (b) charge-discharge curve of $Zn_3V_2O_8$ nanoplatelets, (c) Specific capacity against cycle number and (d) Columbic efficiency against number of cycle.

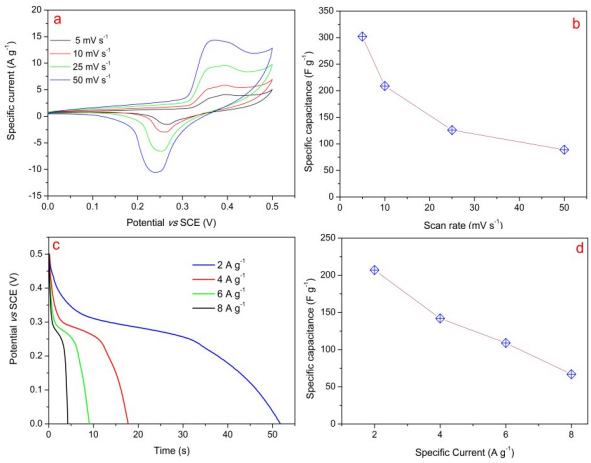

Fig.8. (a) CV curve of $Zn_3V_2O_8$ nanoplatelets, (b) specific capacitance versus scan rate curve, (c) charge-discharge curve of $Zn_3V_2O_8$ nanoplatelets, and (d) specific capacitance versus specific current.

The initial discharge and charge capacities are 752 and 488 mA h g^{-1}, respectively. The irreversible capacity loss of the first cycle is 35.1 %. After the first cycle, the electrochemical process was highly reversible. The discharge and charge capacities of the second cycles are decreased to 558 and 474 mA h g^{-1}, and the capacity loss of second cycle is only 15 %. The irreversible capacity loss of the first cycle may be attributed to lithium loss due to the formation of a solid electrolyte interphase (SEI) layer.[24] Fig. 7c and 7d show the cyclic stability curve and columbic efficiency of $Zn_3V_2O_8$ nanoplatelets. The specific capacity values were decreased from the first cycle to the second cycle, and further large decreases in specific capacity were observed up to the 10th cycle. Thereafter, the specific capacity decreased linearly. The columbic efficiency of $Zn_3V_2O_8$ nanoplatelets increases from the first cycle (64.9 %) to the second cycle (85.1 %), rising to greater than 95 % after the 10th cycle and greater than 99 % at the 40th cycle. Zhang *et al.* [15] synthesized the $Zn_3(VO_4)_2$ microspheres as an anode and reported first and second discharge capacities of 1180 and 676 mA h g^{-1} at a current density of 20 mA g^{-1}. Though the discharge capacities are high, the current density is very low. Gan *et al.*[16] reported a first discharge capacity of 1522 mA h g^{-1} and excellent cyclic stability for $Zn_3V_2O_8$ material. However, they used 30 % conductive material, which likely resulted in a poor specific volumetric capacity.

The electrochemical supercapacitor performance of the $Zn_3V_2O_8$ nanoplatelets was studied using cyclic voltammetry and Galvanostatic charge-discharge studies. The CV study was performed between the potential window of 0 and 0.5 V at different scan rates. Fig.8a depicts the CV curves of the $Zn_3V_2O_8$ nanoplatelet electrode at scan rates of 5, 10, 25, and 50 mV s^{-1}. The shapes of the CV curves do not reveal electric double layer capacitance, indicating that the capacitance is mainly due to pseudocapacitive behavior.[25] CV curves show a pair of redox peaks at about 0.37 and 0.25 V. These redox peaks may originate from the intercalation and de-intercalation of K^+ from the electrolyte into zinc oxide.[26] Fig. S3 shows the scan rate versus peak current curve. It is interesting to note that the variations of peak current with scan rates are linear. This linearity of peak current with scan rate corroborates the electrochemical reaction is surface redox reaction that leads to the pseudocapacitive behavior of the electrode.[27] The specific capacitance, C_c (F g^{-1}) was calculated using the following formula,[28]

$$C_c = \frac{1}{m\nu(V_a - V_c)} \int_{V_a}^{V_c} I(V)dV \qquad 1$$

where, ν is the scan rate, $\Delta V = (V_a - V_c)$ is the potential window, and m is the mass of the electroactive material. The estimated maximum specific capacitance was 302 F g^{-1} at a scan rate of 5 mV s^{-1}. Fig.8b shows the scan rate versus the specific capacitance curve. The specific capacitance decreases when the scan rate is increased from 5 to 50 mV s^{-1}. At high scan rates, the diffusion process limits the movement of K^+ ions into the electrode material. Hence, it intercalates only with the outer surface of the electrode material, resulting in a low specific capacitance. A greater specific capacitance is achieved when the ions diffuse well with the outer and inner surfaces of the electrode materials.[29]

The supercapacitor performance was further evaluated for its specific capacitance and cyclic stability, using charge-discharge analysis. Fig. 8c presents the discharge curves of the $Zn_3V_2O_8$ electrode at different specific currents; 2, 4, 6, and 8 A g^{-1}. The discharge profiles reveal the nonlinear behavior rather than linear behavior of the electric double layer capacitance, suggesting that capacitance is mainly due to pseudocapacitance.[30] The specific capacitance, C_p (F g^{-1}) was calculated using the following formula,[31]

$$C_p = \frac{i\,\Delta t}{m\,\Delta V} \qquad 2$$

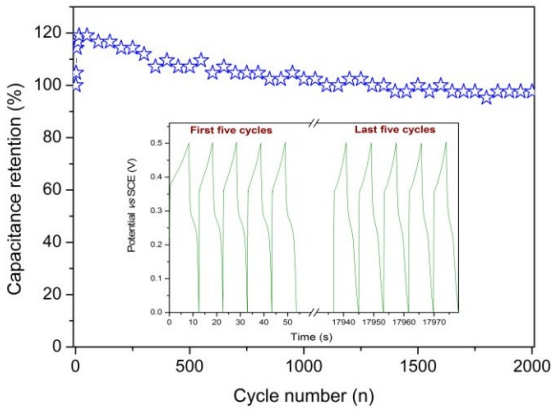

Fig.9. Cyclic stability against number of cycles (Inset shows the initial and final five cycles of charge-discharge)

where, 'i' is the applied specific current, ΔV is the potential window, Δt is the discharge time, and 'm' is the mass of electroactive material. The calculated specific capacitance values were 207, 142, 109, and 67 F g^{-1} at 2, 4, 6, and 8 A g^{-1}, respectively, as presented in fig. 8d. The specific capacitance was greater at a lower specific current. At a low specific current, K^+ ions have sufficient time to intercalate with the inner and outer surfaces of the electrode material, resulting in a higher specific capacitance. However, at a higher specific current, the ions can diffuse only with the outer surface of the electrode material.[32] Hence, specific capacitance decreases with increasing applied specific current. The $Zn_3V_2O_8$ nanoplatelet electrode exhibited a maximum specific capacitance of 302 F g^{-1} at a scan rate of 5 mV s^{-1} and 207 F g^{-1} at a specific current of 2 A g^{-1}. This result is comparable with those previously reported for ZnO and metal vanadate nanomaterials. A ZnO Nanoflake encapsulated carbon nanofiber electrode exhibited a specific capacitance of 216 F g^{-1}, with 94.6 % cyclic stability after 2000 cycles.[33] Butt *et al.* [34] reported the supercapacitor performance of ZnV_2O_4 hierarchical nanospheres. The ZnV_2O_4 nanosphere electrode exhibited a maximum specific capacitance of 360 F g^{-1} at 1 A g^{-1}. Similarly, Shahid *et al.*[35] studied the supercapacitor performance of MoV_2O_8 nanowires, achieving a maximum specific capacitance of 56 F g^{-1} at a scan rate of 5 mV s^{-1}.

Long term cyclic stability is important for practical applications. The long time cyclic stability of the $Zn_3V_2O_8$ electrode was tested over 2000 continuous charge-discharge cycles at a specific current of 8 A g^{-1}. Fig. 9 presents the cyclic stability curve for 2000 cycles. The inset of fig. 9 shows the charge-discharge curve of the first and last five cycles (cycles 1-5 and 1996-2000). The specific capacitance increased from 100 % to 120 % after 15 cycles, decreasing slowly thereafter. After 2000 cycles, about 98 % of the initial specific capacitance was retained. The $Zn_3V_2O_8$ nanoplatelet electrode exhibited good specific capacitance with high cyclic stability. This appreciable performance is mainly due to the crystal structure and morphology of the $Zn_3V_2O_8$ nanoplatelets. The crystal structure of $Zn_3V_2O_8$ is similar to that of $Ni_3V_2O_8$. Three types of O atoms constitute the tetrahedron and octahedron. V is located in the center of tetrahedron and Zn locates in the center of the octahedron.[16] The gap between the octahedron and the tetrahedron, as well as channels of the supercell, allow for a more effective electron and ion transport, leading to an improved electrochemical performance.

Conclusion:

In conclusion, $Zn_3V_2O_8$ nanoplatelets were synthesized by a hydrothermal method using SDS as a surfactant. SDS plays an important role in the control of morphology, acting as a structure directing agent that enhances the growth process to form zinc vanadate platelets. FESEM and HRTEM revealed the nanoplatelets morphology. Battery studies revealed a high discharge capacity at the second cycle (558 mA h g^{-1}). The columbic efficiency was about 99 % at the 40th cycle. Based on CV and charge-discharge measurements, it was shown that the $Zn_3V_2O_8$ nanoplatelets exhibited a maximum specific capacitance of 302 F g^{-1} (5 mV s^{-1}) and 207 F g^{-1} (2 A g^{-1}). The high specific capacitance with excellent cyclic stability confirms the suitability of $Zn_3V_2O_8$ nanoplatelets for supercapacitor applications.

Acknowledgements

This work was supported by the Priority Research Centers Program through the National Research Foundation of Korea (NRF), funded by the Ministry of Education, Science and Technology (MEST) of the Korean government (2009-0093818).

Notes and references

1 P. Simon and Y. Gogotsi, *Nature Mater*, 2008, **7**,845-854
2 C. Yuan, H.B. Wu, Y. Xie and X.W. Lou, *Angew. Chem., Int. Ed*. 2014, **53**, 1488-1504.
3 X. Zhao, B. M. Sanchez, P. J. Dobson and P.S. Grant, *Nanoscale*, 2011, **3**, 839–855.
4 D.P. Dubal, P.Gomez-romero, B.R. Sankapal and R. Holze, *Nano Energy*, 2015, **11**, 377-399.
5 S.G. Mohamed, C-J. Chen, C.K. Chen, S-F. Hu and R-S. Liu, ACS Appl. Mater. Interfaces, 2014, **6**, 22701-22708.
6 W-B. Zhang, L-B. Kong, X-J. Ma, Y-C. Luo and L. Kang, *RSC Adv*., 2014, **4**, 41772-41777.
7 Y. Zhang, Y. Liu, J. Chen, Q. Guo, T. Wang and H. Pang, *Sci. Rep,* 2014, **4**, 5687.
8 F. Cheng and J. Chen, *J. Mater. Chem.,* 2011, **21**, 9841–9848.
9 S. Zhang, R. Hu, Lei Liu and D. Wang, *Mater. Lett.,* 2014, **124**,57-60.
10 L. Xiao, Y. Zhao, J. Yin and L. Zhang, *Chem. Eur. J*. 2009, **15**, 9442-9450.
11 L. Zeng, F. Xiao, J. Wang, S. Gao, X. Ding and M. Wei, *J. Mater. Chem.,* 2012, **22**, 14284-14288.
12 C. Zheng, L. Zeng, M. Wang, H. Zheng and M. Wei, *CrystEngComm*, 2014, **16**, 10309-10313.
13 S. S. Pitale, M. Gohain, I.M. Nagpure , O.M. Ntwaeaborwa, B. C.B. Bezuidenhoudt and H.C. Swart, *Physica B* , 2012, **407**, 1485–1488.
14 R. Shi, Y. Wang, F. Zhou and Y. Zhu, *J. Mater. Chem.,* 2011, **21**, 6313-6320.

15 S. Y. Zhang, X. Xiao, M. Lu and Z.Q. Li, *J Mater Sci,* 2013, **48**, 3679-3685.
16 L-H. Gan, D. Deng, Y. Zhang, G. Li, X. Wang, L. Jiang and C-R. Wang, *J. Mater. Chem. A,* 2014,**2**, 2461-2466.
17 S. Zhang, N. Lei, W. Ma, Z. Zhang, Z. Sun and Y. Wang, *Mater. Lett*., 2014, **129**, 91-94.
18 P. Yang, X. Xiao, Y. Li, Y. Ding, P. Qiang, X. Tan, W. Mai, Z. Lin, W. Wu, T. Li, H. Jin, P. Liu, J. Zhou, C. P. Wong and Z. L. Wang, *ACS nano*, 2013, **7**, 2617-2626.
19 G. Yang, H. Cui, G. Yang and C. Wang, *ACS Nano,* 2014,**8**, 4474-4487.
20 L. Jiang, Y. Qu, Z. Ren, P. Yu, D. Zhao, W. Zhou, L. Wang and H. Fu, *ACS Appl. Mater. Interfaces*, 2015, **7**, 1595−1601.
21 X- F. Lu, D-J. Wu, R-Z. Li, Q. Li, S-H. Ye, Y –X. Tong and G-R. Li, *J. Mater. Chem. A,* 2014, **2**, 4706-4713.
22 L. Z. Pei, N. Lin, T. Wei, H. D. Liu and H. Y. Yu, *J. Alloys Compd,* 2015, **631**, 90-98.
23 F. Wu, C. Yu, W. Liu, T. Wang, J. Feng and S. Xiong, *J. Mater. Chem. A,* 2015, **3**, 16728–16736.
24 S. Zhang, W. An and G. Wu, *Chemical Physics Letters*, 2015, **621**, 1-4.
25 K.K. Purushothaman, I. M. Babu, B. Sethuraman and G. Muralidharan, *ACS Appl. Mater. Interfaces,* 2013, **5**, 10767-10773.
26 X. Dong, Y. Cao, J. Wang, M.B. Chan-park, L. Wang, W. Huang and P. Chen, *RSC Adv.,* 2012, **2**, 4364-4369.
27 S. Vijayakumar, A. K. Ponnalagi, S. Nagamuthu and G. Muralidharan, *Electrochim. Acta*, 2013, **106**, 500– 505.
28 J.W. Lee, A.S. Hall, J-D. Kim and T.E. Mallouk, *Chem. Mater*, 2012, **24**, 1158-1164.
29 P. Justin, S.K. Meher and G.R. Rao, *J. Phys. Chem. C* , 2010, **114**, 5203-5210.
30 S. Vijayakumar, S. Nagamuthu and G. Muralidharan, *ACS Sustainable Chem. Eng.* 2013,**1**, 1110-1118.
31 S. Nagamuthu, S. Vijayakumar and G. Muralidharan, *Energy Fuels,* 2013, **27**, 3508-3515.
32 P. Syedvali, G. Rajeshkhanna, E. Umesh babu, G. U. kiran, G. R. Rao and P. Justin, *RSC Adv.,* 2015, **5**, 38407-38416.
33 S. Shi, X. Zhuang, B. Cheng and X.Wang, *J. Mater. Chem. A,* 2013, **1**, 13779-13788.
34 F. K. Butt, M. Tahir, C. Cao, F. Idress, R. Ahmed, W. S.Khan, Z. Ali, N. Mahmood, M. Tanveer, A. Mahmood and I. Aslam, *ACS Appl. Mater. Interfaces*, 2014, **6**, 13635-13641.
35 M. Shahid, J. Liu, Z. Ali, I. Shakir and M. F. Warsi, *J. Power sources*, 2013, **230**, 277-281.

Graphical abstract:

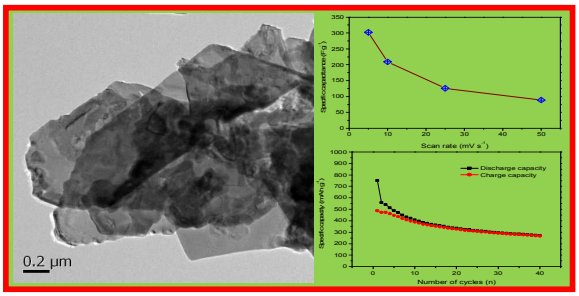

The $Zn_3V_2O_8$ nanoplatelets exhibit maximum specific capacitance of 302 F g^{-1} with 98 % of capacitance retention.